Long-range collisional energy transfer between charge-transfer (ion-pair) states of I2, induced by H2O and I2(X)

Long-range collisional energy transfer between charge-transfer (ion-pair) states of I2, induced by H2O and I2(X)

Trevor Ridley, Kenneth P. Lawley, and Robert J. Donovan

Citation: J. Chem. Phys. **131**, 234302 (2009); doi: 10.1063/1.3272953
View online: http://dx.doi.org/10.1063/1.3272953
View Table of Contents: http://jcp.aip.org/resource/1/JCPSA6/v131/i23
Published by the AIP Publishing LLC.

Long-range collisional energy transfer between charge-transfer (ion-pair) states of I_2, induced by H_2O and $I_2(X)$

Trevor Ridley,[a] Kenneth P. Lawley, and Robert J. Donovan
School of Chemistry, The University of Edinburgh, West Mains Road, Edinburgh EH9 3JJ, Scotland, United Kingdom

(Received 24 September 2009; accepted 19 November 2009; published online 16 December 2009)

Long-range (resonant) energy transfer, between g/u charge-transfer states of molecular iodine [i.e., $f0_g^+(^3P_0) \rightarrow F0_u^+(^3P_0)$ and $E0_g^+(^3P_2) \rightarrow D0_u^+(^3P_2)$], induced by collisions with H_2O and $I_2(X)$ via multipole coupling, has been observed. Large rate constants, up to 5×10^{-9} molecules^{-1} cm^3 s^{-1}, for collisional transfer between a range of vibrational levels of the $f0_g^+(^3P_0)$ and $F0_u^+(^3P_0)$ ion-pair states of I_2, by H_2O, are reported. Some previously reported studies on $E0_g^+(^3P_2) \rightarrow D0_u^+(^3P_2)$ and $f0_g^+(^3P_0) \rightarrow F0_u^+(^3P_0)$ collisional transfer, induced by $I_2(X)$, have been repeated and revised rate data are presented; the range of initially excited vibrational states studied has also been extended. Much smaller rate constants for quenching by $I_2(X)$, compared to H_2O, are found and it is proposed that H_2O desorbed from the walls of the sample cell could have significantly affected much larger rate data previously reported in the literature. For both collision partners, a model is proposed in which long-range, near-resonant interactions can occur when there is close matching of the change in energy in the ion-pair states with the change in energy that accompanies the rotational transition undergone by the collision partner. © *2009 American Institute of Physics*. [doi:10.1063/1.3272953]

I. INTRODUCTION

Our interest in the collisional transfer *between* the ion-pair states of I_2 by H_2O was initiated by an observation that we made in the course of a recent study of amplified spontaneous emission (ASE) from the second tier $f0_g^+(^3P_0)$ ion-pair state.[1] Weak $F0_u^+(^3P_0) \rightarrow X0_g^+$ emission was observed following excitation of the $f0_g^+(^3P_0)$ state by optical-optical double resonance (OODR). It was shown that the preceding $f0_g^+(^3P_0) \rightarrow F0_u^+(^3P_0)$, $g \rightarrow u$, transfer was caused by collisions and not by ASE. Following excitation of $f(v=8)$, emission was observed from F ($v=6$, 7, and 8). Broadly similar results had been reported previously[2] in apparently pure iodine, but the final state vibrational distributions were significantly different in the two studies. One possibility is that a contaminant is present in varying but very small concentrations under the different experimental conditions. These experiments on self-quenching are generally carried out at the vapor pressure of I_2 ($\sim$0.25 Torr) and in order for the presence of a contaminant not to be seen as an increase in background pressure, its rate constant as collision partner for energy transfer would have to be at least one order of magnitude greater than that for $I_2(X)$, so that only trace amounts are required to account for the different results in the literature. In the present study we investigated this phenomenon in more detail and will show that the contradictory results are a likely consequence of varying concentrations of H_2O, desorbed from the walls of the sample cell.

We will also show that H_2O has an equally significant influence on the collisional transfer between the equivalent pair of $\Omega=0$ ion-pair states in the first tier, i.e., $E0_g^+(^3P_2) \rightarrow D0_u^+(^3P_2)$ transfer. Rate constants for collisional transfer by H_2O are measured, and for certain initially excited vibrational levels, found to be up to two orders of magnitude greater than those for collisional transfer by $I_2(X)$. Hence, for these levels, the pressure of H_2O needs only to be one-hundredth of that of $I_2(X)$ to produce equal transfer rates.

There have been several studies on the $E0_g^+(^3P_2) \rightarrow D0_u^+(^3P_2)$ and $f0_g^+(^3P_0) \rightarrow F0_u^+(^3P_0)$ collisional transfer by $I_2(X)$.[2–14] Akopyan *et al.*[2–10] carried out their studies under flow conditions by pumping on an I_2 reservoir and controlling the pressure in the cell by adjusting the entrance and exit flow rates. Ubachs and co-workers[11,12] reported that they evacuated their cell to a pressure below 0.05 Torr. We can only find two studies where special precautions were taken that would definitely have eliminated H_2O. In the first, Fecko *et al.*[13] evacuated their cell to as low as 2×10^{-5} Torr. In the second, Inard *et al.*[14] heated their cell up to 500 °C while evacuating to 10^{-6} Torr and then sublimed I_2 onto the liquid N_2 cooled cell walls. While we have not reproduced these rather stringent conditions, we have been able to carry out some equivalent studies with greatly reduced concentrations of H_2O and the results differ widely from many of those reported in the literature for supposedly pure iodine. It will be proposed that the large rate constants for collisional transfer with H_2O are due to the contribution of large impact parameter collisions that are effective as a result of close matching of the energy changes that accompany the transfer between the ion-pair states of I_2 and dipole-allowed rotational transitions in the ground electronic state of H_2O. A similar proposal is also put forward to account for the relatively few long-range collisional transfers induced by $I_2(X)$ which cannot, in general, provide so many near-resonant channels.

[a]Author to whom correspondence should be addressed. FAX: +44-131-6506453. Electronic mail: t.ridley@ed.ac.uk.

II. EXPERIMENTAL

Known rotational levels ($J=55\pm1$) of various vibrational levels of the $f0_g^+(^3P_0)$ and $E0_g^+(^3P_2)$ states were populated by $(1+1')$ OODR excitation via the intermediate $B0_u^+$ state. In the various excitation schemes, J was varied in order to ensure that the probe laser did not excite another rovibronic level in addition to the rovibrational level of the $f0_g^+(^3P_0)$ or $E0_g^+(^3P_2)$ state of interest. The vibrational level in the intermediate $B0_u^+$ state was chosen so as to give favorable Franck–Condon factors (FCFs) for the probe stage. A XeCl excimer laser (Lambda Physik EMG 201MSC) simultaneously pumped two Lambda Physik dye lasers; an FL 2002 operating with the dyes C153 or C307 and an FL 3002E operating with the dyes PTP and Stilbene 3 (both delivering ~3 mJ per pulse), provided the pump and probe photons, respectively.

The unfocused, counter-propagating, temporally overlapped pump and probe beams were directed through the glass sample cell. The beams crossed at 7° in the emission collection region to prevent any possibility of $f0_g^+(^3P_0) \rightarrow F0_u^+(^3P_0)$ ASE transfer.[1] The emission, at 90° to the laser beams, was dispersed by a Jobin-Yvon HRS2 (f/7, 0.6 m) monochromator and monitored by a Hammamatsu R928 photomultiplier tube. The resolution, determined by the slit widths of the monochromator, was varied; first a wide slit width was used for low resolution survey spectra and for the determination of rate constants, and second narrow slit widths were used, for the higher resolution scans for the determination of vibrational distributions. The slit height was varied to ensure that the intensity of the emission gave a linear response from the photomultiplier. The output from the photomultiplier was processed by a Stanford Research SR250 gated integrator and stored on a personal computer.

The Spectrosil quartz entrance/exit windows for the laser beams were at the Brewster angle. The cell was evacuated with a rotary-backed turbo pump to a base pressure of $<1\times10^{-3}$ Torr as measured by a Pirani gauge on the vacuum manifold. The solid I_2 was held in a side arm of the cell that could be closed to the cell by a tap. All spectra were recorded with I_2 at its vapor pressure, as measured by a 10 Torr MKS baratron gauge connected directly to the cell. H_2O pressures of up to 0.3 Torr were used and the H_2O was degassed and distilled under vacuum before use.

For the studies on collisional transfer by $I_2(X)$, the cell remained open to the I_2 reservoir. For all other studies it was closed and this resulted in the gradual adsorption of I_2 and H_2O, when added, on to the surfaces of the cell during the course of the, typically, 30 min scans. Two measures were taken to counteract this problem. First, the I_2 pressure was allowed to equilibrate to a few mTorr below its vapor pressure before the introduction of the collision partner (for brevity this will still be referred to as the vapor pressure in the text). Second, the total pressure of I_2+H_2O was monitored during each scan and an average pressure determined. This effect leads to errors of around ±5% in the I_2 pressure and up to around ±20% in the lowest H_2O pressures used in the pressure dependence experiments.

Drifts can occur in laser power, wavelength, and spatial overlap during the course of a scan. In order to correct for these drifts, short intensity calibration spectra were recorded both before and after the emission of interest and the intensity ratio was obtained from an average of the two calibration spectra. The estimated uncertainties arising from these drifts are $<\pm10\%$.

III. TREATMENT OF DATA

A. Rate constant calculations

1. Collisional transfer by $I_2(X)$

The treatments used will be described using $f0_g^+(^3P_0) \rightarrow F0_u^+(^3P_0)$ transfer as an example; the equivalent procedures were also used for $E0_g^+(^3P_2) \rightarrow D0_u^+(^3P_2)$ transfer. In the absence of any quenching of the $F0_u^+(^3P_0)$ state to dark states, the full rate equation for collisional transfer by $I_2(X)$ is given by

$$\frac{I_F}{I_f} = \frac{k_3}{k_1}\left[\frac{k_2[I_2]}{k_2[I_2]+k_3}\right], \tag{1}$$

where I_F and I_f are the total integrated fluorescence, in photons s^{-1}, from the $F0_u^+(^3P_0)$ and $f0_g^+(^3P_0)$ states, respectively, and k_1 and k_3 are the reciprocals of the fluorescent lifetimes of the $f0_g^+(^3P_0)$ and state $F0_u^+(^3P_0)$, respectively. k_2 is the rate constant for $f0_g^+(^3P_0) \rightarrow F0_u^+(^3P_0)$ collisional transfer by $I_2(X)$ and it is assumed here that its value is the same for the reverse transfer, $f0_g^+(^3P_0) \leftarrow F0_u^+(^3P_0)$.

When the pressure is low enough for the rate of the back reaction $f0_g^+(^3P_0) \leftarrow F0_u^+(^3P_0)$ to be negligible (single collision conditions) the rate equation can be simplified to

$$\frac{I_F}{I_f} = \frac{k_2[I_2]}{k_1}. \tag{2}$$

Judging from the values of k_2 to be presented, the vapor pressure of I_2, ≤0.3 Torr, always lies in the single collision regime ($k_2[I_2]/k_3$ is ≤0.1) for the present studies and all values of k_2 were obtained at this single pressure and calculated using Eq. (2).

$I_{F\rightarrow X}$ and $I_{f\rightarrow B}$ were obtained from the observed $F0_u^+(^3P_0) \rightarrow X0_g^0$ and $f0_g^+(^3P_0) \rightarrow B0_u^+$ emissions, respectively. The observed spectra were first corrected for the response function of the detector and then converted to units of photons s^{-1} and all of the spectra shown have been corrected in this way. The corrected spectra were then integrated using a commercial software package. The corrected intensities of the observed emission systems were then divided by the appropriate I_{ik}, the integrated fluorescence intensity of the transition $i\rightarrow k$ relative to the total fluorescence, to obtain I_F and I_f.

In the present experiments, (I_F/I_f) could be <0.01. With our detection system, there is an inherent problem associated with accurately measuring the relative integrated intensities of two emission systems that differ by two or more orders of magnitude. The magnitude of the fluorescence of the weak system must be large enough for the signal-to-noise ratio to be such that an accurate integrated intensity can be measured, while ensuring that it is not too large for partial saturation of the detection system to occur for the strong emis-

sion. In order to circumvent this problem, a two or three step method was used which involved the use of emissions with an intermediate intensity. In both methods, the ratio of the entire $F0_u^+(^3P_0) \rightarrow X0_g^+$ emission intensity to that of two or three weak bands at the blue end of the $f0_g^+(^3P_0) \rightarrow B0_u^+$ emission was obtained from spectra recorded with good signal-to-noise levels. This ratio was determined either directly or using part or all of the $f0_g^+(^3P_0) \rightarrow C1_u$ and $f0_g^+(^3P_0) \rightarrow A1_u$ emission (see Sec. IV) as an intermediate intensity calibration. The percentage contribution that the three $f0_g^+(^3P_0) \rightarrow B0_u^+$ vibronic bands make to the total $f0_g^+(^3P_0) \rightarrow B0_u^+$ emission was then calculated from the FCFs, corrected for the wavelength and transition dipole dependencies.

2. Collisional transfer by H_2O

(I_F/I_f) observed in the presence of H_2O is given by

$$\frac{I_F}{I_f} = \frac{k_3}{k_1}\left[\frac{k_4[H_2O] + k_2[I_2]}{k_4[H_2O] + k_2[I_2] + k_3}\right], \tag{3}$$

where k_4 is the rate constant for $f0_g^+(^3P_0) \rightarrow F0_u^+(^3P_0)$ collisional transfer by H_2O and also for the reverse transfer. Single collision conditions are now defined as being achieved when the ratio $(k_2[I_2]+k_4[H_2O])/k_3$ is ≤ 0.1. Under these conditions, Eq. (3) can be simplified to

$$\frac{I_F}{I_f} = \frac{k_2[I_2]}{k_1} + \frac{k_4[H_2O]}{k_1}. \tag{4}$$

With one exception, k_4 for $f0_g^+(^3P_0) \rightarrow F0_u^+(^3P_0)$ transfer was obtained at a single combination of I_2 ($\sim$0.25 Torr) and H_2O ($\sim$0.06 Torr) pressures that always lies in the single collision regime for the vibrational levels studied. Using the value of k_2 found by the procedure in Sec. III A 1, k_4 was then calculated from the observed ratio I_F/I_f using Eq. (4). The equivalent procedure was used for $E(v=9)$. The same combination of pressures did not lie in the single collision regime for $E(v=13)$, hence k_4 was obtained from Eq. (3). For $f(v=7)$ and $E(v=8)$, (I_F/I_f) was measured as a function of H_2O pressure and k_4 obtained from Stern–Volmer plots.

3. Uncertainty limits

Both random and systematic errors contribute to the overall uncertainty limits attached to the absolute values of k_2 and k_4 for $I_2(X)$ and H_2O as collision partners. An estimate of the random errors can be derived from the error in the slopes of the Stern–Volmer plots ($<$10%). Several factors common to both sets of measurements give rise to systematic errors. First, we neglected the small unrecorded contribution to I_F from the transition to the shallow bound 0_g^+ valence state that dissociates to two $I(^2P_{1/2})$ atoms; had this been included the derived values of k_2 and k_4 would have increased slightly. Second, there are errors associated with the literature values of I_{ik}, the $F0_u^+(^3P_0) \rightarrow X0_g^+$ and $f0_g^+(^3P_0) \rightarrow B0_u^+$ transition dipoles, the lifetime of the $f0_g^+(^3P_0)$ state [only the value for $f(v=0)$ is reported] and the detector response function. Thus, the overall uncertainty limits in the absolute values of k_2 and k_4, random plus systematic, could be as high as $\pm$30%. However, the key point for this paper is that both k_2 and k_4 move in tandem as a result of the systematic errors and thus any conclusions we will make about the relative quenching efficiency of $I_2(X)$ and H_2O are unaffected.

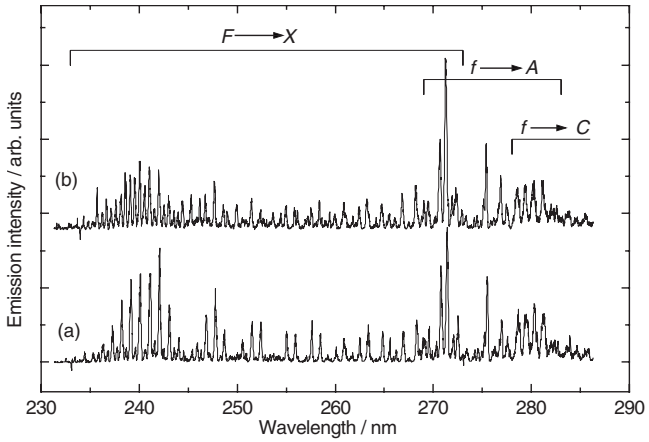

FIG. 1. The $F0_u^+(^3P_0) \rightarrow X0_g^+$ ($\lambda \leq 273$ nm) and part of the $f0_g^+(^3P_0) \rightarrow A1_u$ and $f0_g^+(^3P_0) \rightarrow C1_u$ ($\lambda \geq 273$ nm) emissions following excitation of $f(v=12)$ recorded (a) immediately after refilling the cell and (b) 20 h later. The intensities of the spectra are normalized to the $f0_g^+(^3P_0) \rightarrow C1_u$ and $f0_g^+(^3P_0) \rightarrow A1_u$ emissions.

B. Final state vibrational distributions

1. Collisional transfer by $I_2(X)$

The two lobes of intensity at the blue end of the $F0_u^+(^3P_0) \rightarrow X0_g^+$ emission were recorded under higher resolution (see Figs. 1 and 2). This region always contains several fully resolved bands from single vibrational levels of the upper state. The relative intensities of these bands were simulated from FCFs, corrected for the wavelength and transition dipole dependencies, from which the relative contributions of each upper state vibrational level, $N_v(I_2)$, were obtained.

2. Collisional transfer by H_2O

The relative contributions of each upper state vibrational level in the spectrum recorded in the presence of H_2O, $N_v(\text{total; } I_2+H_2O)$, were obtained as above. Knowing k_2, k_4, $[I_2]$, and $[H_2O]$, $N_v(I_2)$ can be calculated and subtracted from $N_v(\text{total})$ to give the contributions due to collisions with H_2O, $N_v(H_2O)$. The percentage error associated with N_v depends on the magnitudes of N_v, k_2, and k_4 and the efficiency with which the $f0_g^+(^3P_0)$ state vibrational level can be excited and varies between $\pm$5% for large N_v and $\pm$50% for small N_v.

C. Calculation of FCFs

FCFs, taken to be $\langle fv'|\mu_{fF}(R)|Fv''\rangle^2$ in this paper, were calculated using potentials generated from well known molecular constants or from RKR points.[15–20] Transition dipole functions reported by Akopyan *et al.*[21,22] were used.

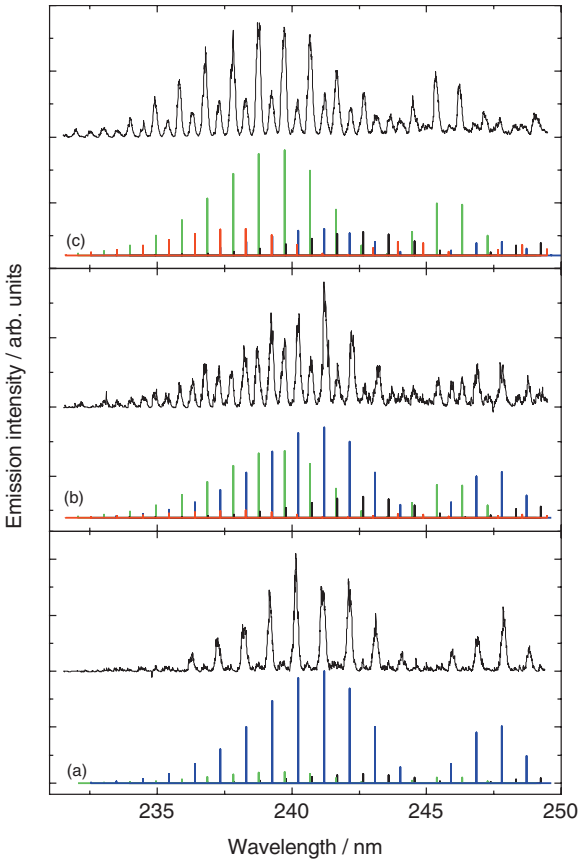

FIG. 2. Part of the $F0_u^+(^3P_0) \rightarrow X0_g^+$ emission following excitation of $f(v=12)$ recorded (a) immediately after refilling the cell, (b) 20 h later, and (c) with I_2(0.28 Torr)+H_2O(0.14 Torr). In the stick spectra (simulation) in (a), (b), and (c) N_{10}(black):N_{11}(blue):N_{12}(green):N_{13}(red) are 0.08:1:0.1:0, 0.2:1:0.7:0.1 and 0.2:0.2:1:0.2, respectively.

IV. RESULTS

A. Changes in $F0_u^+(^3P_0)$ and $D0_u^+(^3P_2)$ state fluorescence with cell residence time

1. Excitation of $f(v=12)$

Fluorescence from the $F0_u^+(^3P_0)$ state was observed to change slowly with the time interval after filling the cell. The spectrum recorded following excitation of $f(v=12)$ immediately after the cell had been evacuated and refilled with I_2 is shown in Fig. 1(a). The emission below 273 nm is $F0_u^+(^3P_0) \rightarrow X0_g^+$ following collision-induced $f0_g^+(^3P_0) \rightarrow F0_u^+(^3P_0)$ transfer, while that above 273 nm is a combination of direct $f0_g^+(^3P_0) \rightarrow C1_u$ and $f0_g^+(^3P_0) \rightarrow A1_u$; a small fraction of the latter system also extends down to ~269 nm. A slower scan of the blue end of the $F0_u^+(^3P_0) \rightarrow X0_g^+$ emission is shown in the upper trace of Fig. 2(a). Stick spectra of the positions and FCFs for the $(J'=55) \rightarrow (J''=55)$ transitions of the various $F0_u^+(^3P_0) \rightarrow X0_g^+$ vibronic bands with $v=10$, 11, 12, and 13 in the upper state are also shown. The relative populations of the $F0_u^+(^3P_0)$ levels $N_{10}:N_{11}:N_{12}:N_{13}$, immediately after filling the cell, are 0.08:1:0.1:0. This contrasts with the relative populations of 0.2:1:0.7:0.1 for the same four levels reported in the literature.[2]

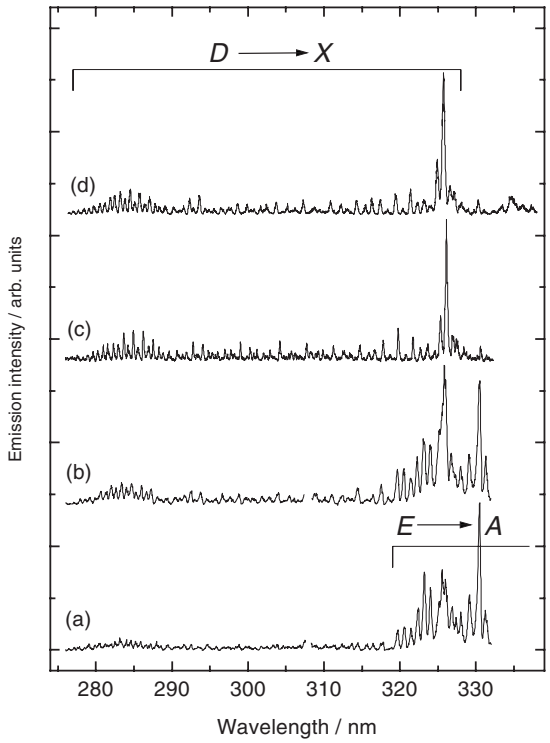

FIG. 3. Emission between 275 and 333 nm following the excitation of $E(v=8)$ recorded (a) immediately after refilling the cell, (b) 3 h later, (c) in an earlier study (Ref. 23), and (d) with 0.03 Torr of H_2O added. The intensities of the spectra are normalized to the most intense peaks. The $D0_u^+(^3P_2) \rightarrow X0_g^+$ emission extends from ~275–328 nm.

The spectrum shown in the upper trace of Fig. 2(b) was recorded 20 h after the cell had been refilled and the tap to the reservoir closed. Clearly, the vibrational distributions in the $F0_u^+(^3P_0)$ state have changed as a function of time. A stick spectrum simulation of the spectrum recorded after 20 h is shown in the lower trace of Fig. 2(b) in which $N_{10}:N_{11}:N_{12}:N_{13}$ are 0.2:1:0.7:0.1, the same as those reported previously.[2]

The spectrum shown in Fig. 1(b) also recorded after 20 h does indeed appear to reproduce quite accurately, albeit at higher resolution, the spectrum shown in Fig. 2(b) of Ref. 2. The literature spectrum was recorded from a higher rotational level but it was reported[2] that the vibrational distributions did not vary with J. The observed vibrational distributions strongly suggest that the cell used in the previous study had an ever-present impurity and that we can remove the same impurity from our cell for a short time by re-evacuating the cell.

2. Excitation of $E(v=8)$

In order to see if the same effect is observed for $E0_g^+(^3P_2) \rightarrow D0_u^+(^3P_2)$ collisional energy transfer, i.e., the equivalent process in the first tier of ion-pair states, we recorded the $D0_u^+(^3P_2) \rightarrow X0_g^+$ emission following excitation of $E(v=8)$ immediately after refilling the cell and 3 h later and these spectra are shown in Figs. 3(a) and 3(b). With the exception of part of the broad band around 325 nm, all of the emission above 320 nm in the spectrum in Fig. 3(a) is due to $E0_g^+(^3P_2) \rightarrow A1_u$. Very weak $D0_u^+(^3P_2) \rightarrow X0_g^+$ emission is

observable between 275 and 320 nm. The intensity of the $D0_u^+(^3P_2) \rightarrow X0_g^+$ relative to the $E0_g^+(^3P_2) \rightarrow A1_u$ is greater in the spectrum recorded after 3 h, consistent with significant concentrations of impurity being present in this period. The spectrum in Fig. 3(c) was recorded in one of our earlier studies[23] where we were unaware of the problem. Here, the $D0_u^+(^3P_2) \rightarrow X0_g^+$ emission is now an order of magnitude more intense than the $E0_g^+(^3P_2) \rightarrow A1_u$ emission indicating an even larger concentration of impurity. The spectrum shown in Fig. 3(c) also resembles that shown in Fig. 1(a) of Ref. 9. Thus, it can be concluded that the transfer between both g/u pairs of states is affected to a similar extent by an impurity that is common to at least two research groups.

B. Identification of the impurity

Having shown that there is some impurity being desorbed from the surfaces of the cell as a function of time, the next step was to identify it. Separate experiments were therefore conducted with low added pressures of N_2, air, and H_2O. From this work it was immediately clear that H_2O was by far the most efficient energy transfer agent and we will show that the above observations are entirely consistent with H_2O being the impurity by adding known pressures of water vapor. We will also show theoretically that water has the required properties to produce very large parity changing collision rates. From a practical point of view, water is of course well known to be adsorbed on glass and difficult to remove.

Four facts should be emphasized at this point. First, during the 20 h over which the spectra in Fig. 1 were recorded, there was no observable change in the pressure in the cell that was greater than the variation in the vapor pressure of I_2 with changing room temperature and/or absorption of I_2 on to the cell walls, i.e., ± 0.02 Torr. Second, the cell was thoroughly leak tested. Third, the cell and the reservoir had not been exposed to air for approximately six months prior to obtaining these data. Finally, the initial observations were made before any H_2O had been deliberately introduced into the cell, i.e., any water in the cell or sample could be described as residual.

1. Observations following excitation of $f(v=12)$

The blue end of the $F0_u^+(^3P_0) \rightarrow X0_g^+$ emission following excitation of $f(v=12)$ observed from I_2 (vapor pressure) +0.14 Torr H_2O is shown in Fig. 2(c). We will show subsequently that with this combination of I_2 and H_2O pressures that ~90% of the $F0_u^+(^3P_0) \rightarrow X0_g^+$ emission is due to collisions with H_2O. In this spectrum, $N_{10}:N_{11}:N_{12}:N_{13}$ are 0.2:0.2:1:0.2. It can be seen that the bands whose relative intensities are greater in Fig. 2(b) than in Fig. 2(a), e.g., from $v=12$, are those that are most intense in Fig. 2(c).

2. Observations following excitation of $E(v=8)$

Two sections of the $D0_u^+(^3P_2) \rightarrow X0_g^+$ emission following excitation of $E(v=8)$ are shown in Fig. 4: I_2 (vapor pressure) recorded with a freshly refilled cell [Figs. 4(a) and 4(c)] and with 0.065 Torr of H_2O added [Figs. 4(b) and 4(d)]. The

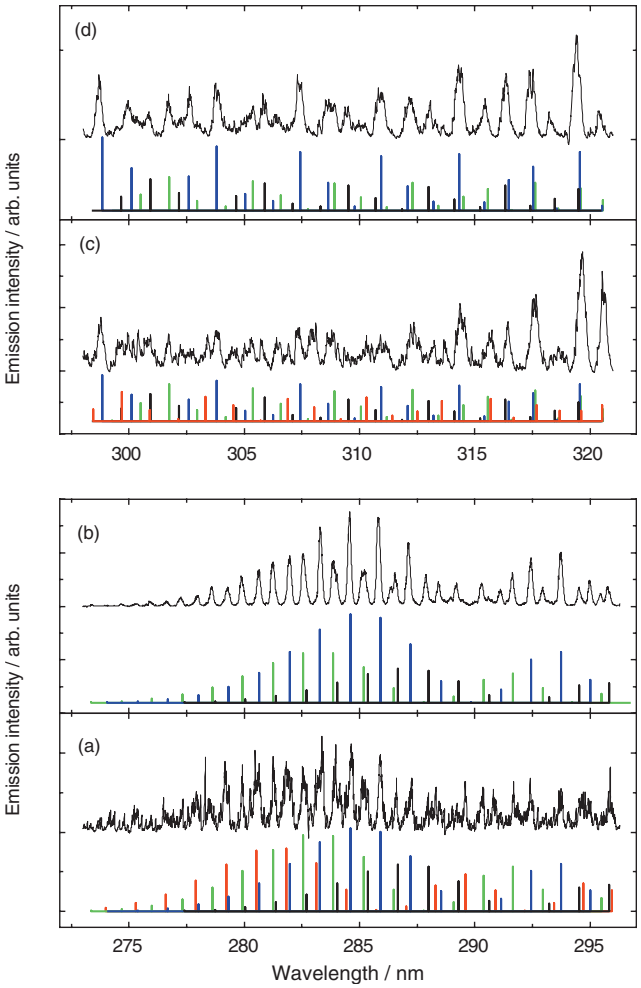

FIG. 4. Two sections of the $D0_u^+(^3P_2) \rightarrow X0_g^+$ emission following excitation of $E(v=8)$ recorded [(a) and (c)] immediately after refilling the cell and [(b) and (d)] with 0.065 Torr of H_2O added. The intensities of the two spectra in each section are normalized to the most intense peaks. The spectra in (c) and (d) were recorded with lower resolution. In the stick spectra (simulation) in (a) and (c) N_{10}(black):N_{11}(blue):N_{12}(green):N_{13}(red) are 0.5:1:0.9:0.6 while in (b) and (d) they are 0.4:1:0.5:0.

spectra shown in Figs. 4(c) and 4(d) were recorded with lower resolution than in Figs. 4(a) and 4(b). In the stick spectra in Figs. 4(a) and 4(c), $N_{10}:N_{11}:N_{12}:N_{13}$ are 0.5:1:0.9:0.6 while in Figs. 4(b) and 4(d) they are 0.4:1:0.5:0. The ratios used to simulate the spectra in Figs. 4(b) and 4(d), i.e., with H_2O added, are the same as those used by Akopyan *et al.*[9] to simulate the spectrum that they observed following excitation of $E(v=8)$ but slightly different from the ratios of 0.3:1:0.3:0 reported by the same group in an earlier study.[5] The spectrum shown in Fig. 4(d) reproduces that shown in Fig. 4 of the earlier study.[5]

Overall, it is concluded that the results for both the $f0_g^+(^3P_0)$ and $E0_g^+(^3P_2)$ states are consistent with the impurity being water. As noted above, in the experiment in which the cell was left for 20 h and appreciable quenching by H_2O is observed, there was no significant change in the pressure gauge. These observations show that the rate constant for collisional transfer by H_2O is large relative to that for transfer by $I_2(X)$.

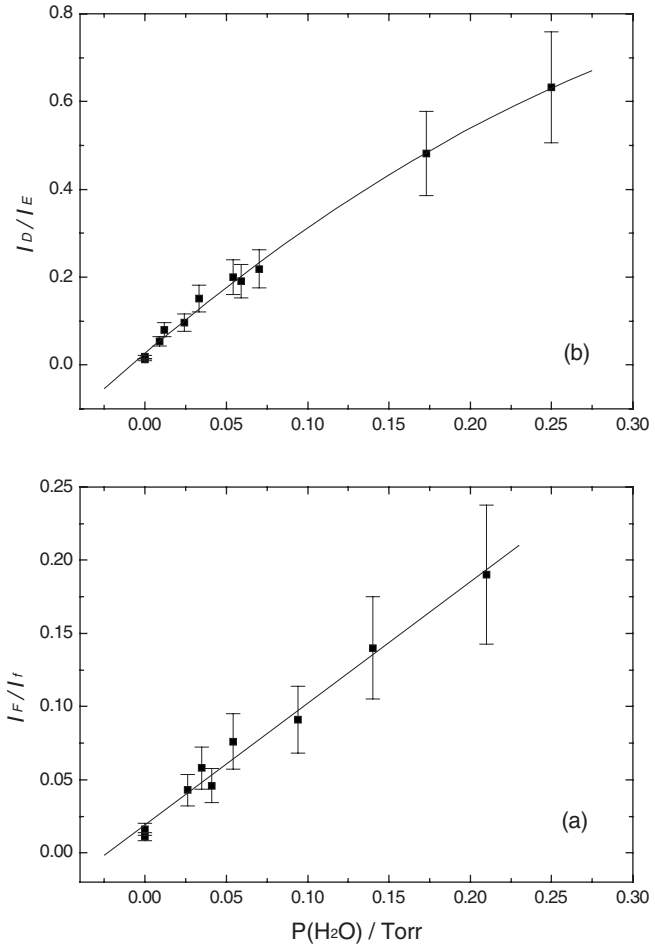

FIG. 5. (a) A plot of I_F/I_f against the pressure of H_2O added following excitation of $f(v=7)$ and (b) a plot of I_D/I_E against the pressure of H_2O added following excitation of $E(v=8)$.

C. Vibrational distributions and total rate constants determined for the collisional transfer from various vibrational levels of the $f0_g^+(^3P_0)$ and $E0_g^+(^3P_2)$ states by H_2O

1. Collisional transfer from $f(v=7)$

For $f(v=7)$, the integrated intensities of the $F0_u^+(^3P_0) \rightarrow X0_g^+$, $(I_{F\rightarrow X})$ and $f0_g^+(^3P_0) \rightarrow B0_u^+$, $(I_{f\rightarrow B})$ emissions were measured for I_2 (vapor pressure) with seven added pressures of H_2O in the range 0.03–0.21 Torr. $(I_{f\rightarrow B})$ was taken to be the same as I_f and $(I_{F\rightarrow X})$ was converted to I_F by dividing by 0.91.[24] A plot of I_F/I_f against the pressure of H_2O is shown in Fig. 5(a). The plot is linear confirming that we are working in the single collision regime as defined above. Inserting the gradient of the plot into Eq. (4) and using a lifetime of 14 ns for the $f0_g^+(^3P_0)$ state[24] gives a rate constant, k_4, of 20×10^{-10} molecules^{-1} cm^3 s^{-1}.

2. Collisional transfer from $E(v=8)$

For $E(v=8)$, the integrated intensities of the $D0_u^+(^3P_2) \rightarrow X0_g^+$, $(I_{D\rightarrow X})$ and $E0_g^+(^3P_2) \rightarrow B0_u^+$, $(I_{E\rightarrow B})$ emissions were measured with nine different pressures of H_2O in the range 0.015–0.25 Torr. For the lowest pressures, the total integrated intensity of the $D0_u^+(^3P_2) \rightarrow X0_g^+$ emission was obtained by measuring the part below 320 nm and scaling it up using a factor (~1.7) derived from the highest pressure spectrum. This was necessary because the part above 320 nm is obscured by $E0_g^+(^3P_2) \rightarrow A1_u$ in the low pressure spectra. It is assumed that the scaling factor remains constant with pressure. $I_{E\rightarrow B}$ was taken to be the same as I_E and $I_{D\rightarrow X}$ was converted to I_D by dividing by 0.83.[1]

The plot of I_D/I_E against the pressure of H_2O shown in Fig. 5(b) is clearly not linear. The gradient of the limiting slope at low pressures, determined from a quadratic fit of the full data set, was not significantly different from the gradient of a linear fit of the data with pressures of ≤0.07 Torr. Again, this is consistent with the estimate of the single collision limit defined above. Inserting the initial gradient of the plot into Eq. (4) and using a lifetime of 26 ns for the $E0_g^+(^3P_2)$ state,[24,25] gives $k_4=35 \times 10^{-10}$ molecules^{-1} cm^3 s^{-1}. This value of k_4 for the excited level is two orders of magnitude greater than that obtained for the transfer by $I_2(X)$, k_2, for the same level (see below). Consequently, only 2 mTorr of H_2O is required to produce approximately the same intensity of collision-induced emission as 0.2 Torr of I_2.

3. Other vibrational levels

The vibrational distributions and rate constants for the collisional transfer from f ($v=2-12$ and 14) and E ($v=8$, 9 and 13) by H_2O are presented in Tables I and II, respectively. The rate constants for the $f0_g^+(^3P_0)$ state as a function of v are also shown as a plot in Fig. 6.

D. Vibrational distributions and rate data for the collisions with $I_2(X)$

1. Collisional transfer from $f(v=2-12$ and 14)

Vibrational distributions and rate constants for the collisional transfer from $f(v=8-19)$ to $F(v)$, by $I_2(X)$, were reported by Akopyan *et al.*[2] We have shown above that this study was probably influenced by the presence of residual H_2O. While we cannot claim to be able to totally remove H_2O from our cell, we are now in a position to minimize it by recording spectra within 1 h of refilling the cell. Consequently, we repeated some of the earlier work and extended the range down to $v=2$.

The $F0_u^+(^3P_0)$ state vibrational distributions observed following collisional transfer from f ($v=2-12$ and 14) by $I_2(X)$ are presented in Table I. In all of the vibrational distributions reported previously,[2] $v=8-10$, 12, 14, and 17, the most intense emission was observed from the vibrational level of the $F0_u^+(^3P_0)$ state nearest in energy to the initially excited level. Furthermore, it was concluded that the $f0_g^+(^3P_0) \rightarrow F0_u^+(^3P_0)$ collisional transfers could be separated into two groups; (i) "near resonant" where the energy mismatch between the initially excited level and the nearest vibrational level of the $F0_u^+(^3P_0)$ state, ΔE_{I_2}, is between 0 and 25 cm^{-1} and (ii) "nonresonant" where ΔE_{I_2} is >25 cm^{-1}.

The present data support this conclusion for the vibrational levels common to both studies and additionally for $v=2$ and 11. In all of the near-resonant examples examined here, the intensity of the emission from the vibrational level

TABLE I. Vibrational level distributions, N_v, for the $F0_u^+(^3P_0)$ state, (F_v), and $D0_u^+(^3P_2)$ state, (D_v), observed following transfer from various levels of the $f0_g^+(^3P_0)$ state, (f_v), and $E0_g^+(^3P_2)$ state, (E_v), respectively, by collisions with $I_2(X)$ and H_2O. FCFs, and energy gaps, ΔE_{I_2}, for the transitions from $J=55 \rightarrow J=54/56$ are also given.

				N_v		
				$I_2(X)$		
f_v	f_v	ΔE_{I_2} $(J''=54/56)/cm^{-1}$	FCF		Lit.[a]	H_2O
2	0	22.5/18.0	0.002	1		0.1
	1	−72.9/−77.5	0.060	0.04		1
	2	−167.5/−172.0	0.854	0.04		0.5
3	1	29.8/25.2	0.006	1		0.1
	2	−64.8/−69.3	0.069	<0.1		1
	3	−158.4/−163.0	0.836			0.7
4	2	37.5/33.0	0.010	1		0.1
	3	−56.1/−60.7	0.067	0.10		1
	4	−148.9/−153.4	0.835	0.10		0.6
5	3	45.8/41.2	0.015	1		0.3
	4	−47.0/−51.5	0.058	0.07		0.9
	5	−138.8/−143.4	0.844	0.06		1
6	4	54.5/50.0	0.021	1		0.3
	5	−37.3/−41.9	0.046	0.2		1
	6	−128.3/−132.8	0.857	0.1		1
7	5	63.7/59.1	0.027	1		0.5
	6	−27.3/−31.8	0.032	0.6		0.5
	7	−117.3/−121.9	0.869	0.2		1
8	6	73.4/68.9	0.034	0.2	0.5	0.6
	7	−16.7/−21.2	0.020	1	1	0.6
	8	−106/−110.5	0.871	0.1	0.9	1
9	7	83.5/79.0	0.042	0.04	0.1	0.4
	8	−5.8/−10.3	0.010	1	1	0.1
	9	−94.3/−98.9	0.857	0.05	0.7	1
	10	−182.1/−186.7	0		0.2	
10	8	94.0/89.5	0.050	0.02	0.3	0.5
	9	5.5/0.9	0.003	1	1	0
	10	−82.3/−86.9	0.822	0.02	0.6	1
11	9	104.9/100.3	0.059	0.02		0.5
	10	17.1/12.5	0.0005	1		0.1
	11	−70.0/−74.6	0.763	0.04		1
	12	−156.5/−161.0	0.042			0.1
12	10	116.1/111.5	0.066	0.1	0.2	0.2
	11	29.0/24.4	0.0001	1	1	0.1
	12	−57.5/−62.0	0.682	0.1	0.7	1
	13	−143.4/−147.9	0.100		0.1	0.2
14	12	139.2/134.7	0.074	0.1	0.3	0.2
	13	53.3/48.8	0.002	0.7	0.3	0.1
	14	−32.0/−36.6	0.472	1	1	1
	15	−116.9/−121.5	0.284	0.1	0.4	0.4
E_v	D_v				Lit.[b]	
8	10	247.1/242.6	0.344	0.5	0.3	0.4
	11	154.8/150.3	0.210	1	1	1
	12	62.7/58.2	0.021	0.9	0.3	0.5
	13	−29.1/−33.6	0.0001	0.6		
9	11	252.4/247.9	0.307	0.2	0.6	1
	12	160.3/155.8	0.252	0.4	0.6	1
	13	68.5/64.0	0.032	0.4	0.6	1
	14	−23.1/−27.6	0.0003	1	1	0.2
13	15	272.4/268.0	0.105			0.3
	16	181.4/176.9	0.367		0.1	0.9
	17	90.6/86.2	0.105	0.03	0.1	1
	18	0.1/−4.3	0.003	1	1	

[a]Reference 2.
[b]Reference 5.

with the smallest ΔE_{I_2} is always at least ten times more intense than that from the next nearest level. In the remaining levels, $v=3-7$, the vibrational distribution is more evenly spread and the greatest intensity is not always observed from the level with the smallest ΔE_{I_2}.

The rate constants observed for collisional transfer from f ($v=2-12$ and 14) by $I_2(X)$ are presented in Table II and shown as a plot in Fig. 6. Significant enhancement of the rate constants of the near-resonant $v=8-12$ levels are observed as reported previously.[2] However, there is no significant enhancement of $v=2$ which also just qualifies for the near-resonant category. Some literature[2] values that are approximately five times greater than ours are also included in Fig. 6. The presence of residual H_2O in the earlier study probably explains some of the discrepancy between the two data sets.

Although we have been able to significantly reduce the concentration of H_2O in the cell, it is possible that some remaining trace amounts can still influence the observed vibrational distributions and rate constants. This is particularly true for those levels ($v=3-7$) that are not in near resonance with an $F0_u^+(^3P_0)$ state level and hence have very small rate constants for transfer with $I_2(X)$, especially relative to those for H_2O transfer from the same level. However, in none of the spectra from these five levels does the most intense vibrational band correspond to the most intense band in the same spectrum recorded in the presence of H_2O. Therefore, it is concluded that, for these four levels, the majority of the $f0_g^+(^3P_0) \rightarrow F0_u^+(^3P_0)$ transfer is still due to collisions with $I_2(X)$ rather than with H_2O.

TABLE II. Rate constants, in units of 10^{-10} molecules^{-1} cm^3 s^{-1}, for transfer from various levels of the $f0_g^+(^3P_0)$ state, (f_v), and $E0_g^+(^3P_2)$ state, (E_v), by collisions with $I_2(X)$ and H_2O.

	$I_2(X)$			
f_v	Lit.[a]			H_2O
2	0.9			15
3	1.2			13
4	1.3			15
5	0.9			16
6	0.7			20
7	0.9			20[b]
8	2.1	10		26
9	4.8	20		29
10	8.0	24		29
11	4.3	18		34
12	2.6	12		47
14	1.6	10		50
E_v		Lit.[c]	Lit.[d]	
8	0.2	7.1	4.0	35[b]
9	0.4	8.5		31
13	5.5	45	14	43

[a]Reference 2.
[b]Value obtained from pressure dependence measurements.
[c]Reference 5.
[d]Reference 9.

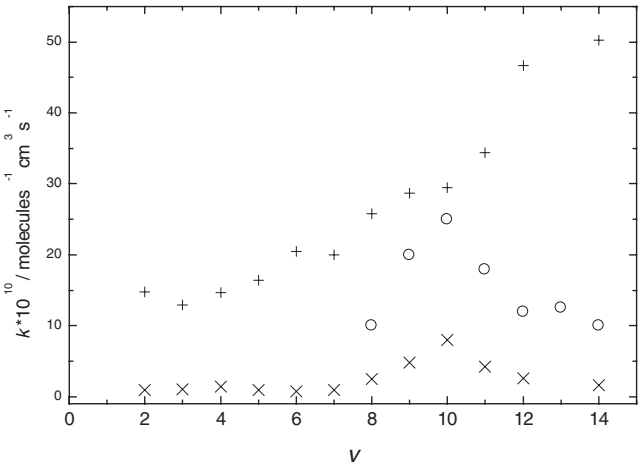

FIG. 6. The rate constants for collisional transfer from f ($v=2-12$ and 14): "×" $I_2(X)$ present data, "○" $I_2(X)$ literature data (Ref. 2), and "+" H_2O present data.

2. Collisional transfer from E(v=8, 9, and 13)

The $D0_u^+(^3P_2)$ state vibrational distributions and rate constants for collisional transfer from E ($v=8$, 9, and 13) by $I_2(X)$ are presented in Table I. The results are in broad agreement with those of two earlier studies,[5,9] but, as for the $f0_g^+(^3P_0) \rightarrow F0_u^+(^3P_0)$ transfer, the contrast between the near-resonant level, $v=13$, and the nonresonant level, $v=8$, is more distinct. In particular, we find that the rate constant for the near-resonant level is ~25 times greater than that for the nonresonant level while the previous studies showed it to be only approximately six and three times greater.[5,9]

V. DISCUSSION

A. Model for the collisional transfer

1. H_2O

Surveying the results for collisional transfer from the $f0_g^+(^3P_0)$ state in Tables I and II, it is seen that self-quenching leads to rates of $k_2 \sim 1 \times 10^{-10}$ molecules^{-1} cm^3 s^{-1}, peaking weakly at $v=10$ when k_2 rises to 8×10^{-10} molecules^{-1} cm^3 s^{-1}. With H_2O as the collision partner, k_4 rises monotonically from 13×10^{-10} molecules^{-1} cm^3 s^{-1} to 50×10^{-10} molecules^{-1} cm^3 s^{-1}. The accompanying vibrational state distributions are also very different for the two collision partners. With $I_2(X)$, the transition involving the smallest energy change in the ion-pair state dominates, even at the expense of a very small FCF, but with H_2O, achieving a good FCF plays a vital role even if relatively large (≥ 100 cm^{-1}) vibrational energy changes are the consequence. We will now show that these differences between the two collision partners can be explained by the wide range of dipole-allowed rotational transitions that H_2O can use to achieve overall internal energy matching.

The rate constants for $I_2(X)$ as partner (apart from the weakly resonant cases) correspond to small impact parameter collisions with b values of gas kinetic dimensions, up to ~4 Å, for an average collision velocity of 2×10^4 cm s^{-1}. Motion over a four-body potential surface would be necessary to describe the outcome of these collisions. With H_2O as

partner, a rate constant of 20×10^{-10} molecules^{-1} cm^3 s^{-1} would imply that, with a mean relative velocity of 6×10^4 cm s^{-1}, collisions with $b\geq10$ Å are responsible if transfer to a single final vibrational state is dominant. The rate constants for individual vibronic transitions $f(v')\rightarrow F(v'')$ are obtained by partitioning the total $g\rightarrow u$ rate according to the observed final vibrational state distribution. The maximum rate we observed, from $f(v=14)$, is 50×10^{-10} molecules^{-1} cm^3 s^{-1} and the rate constant for the dominant channel, $f(v=14)\rightarrow F(v=14)$, is thus 30×10^{-10} molecules^{-1} cm^3 s^{-1}, implying that transition probabilities for collisions with impact parameters $\lesssim12$ Å must be high. However, this assumes that every rotational state of water is equally effective.

We propose that specific rotational transitions in H_2O are required for good energy matching with the observed vibrational changes in the ion-pair state. In that case, only a fraction $W_{v'v''}$ of the total population of water molecules can contribute to a given $(v')\rightarrow(v'')$ transition and the detailed rate constant for these states is $k(v'v'')/W_{v'v''}$. We will see below that these resonant rotational states of water, which differ for each vibrational channel, comprise no more than ~20% of the population and so the maximum detailed rate constants we have to account for are up to $\sim150\times10^{-10}$ molecules^{-1} cm^3 s^{-1}. This implies that b values ~30 Å can lead to appreciable transition probabilities, with $b\sim20$ Å being required for many of the channels where the detailed rate constants are $\sim100\times10^{-10}$ molecules^{-1} cm^3 s^{-1}. Is this feasible?

For large impact parameter collisions to be effective, the long-range coupling between the transition dipole and the leading permanent multipole moment in the collision partner must be responsible, as has been recognized for some time.[26] Dipole-dipole coupling has been used in a model for vibronic relaxation in the $\tilde{A}$ and $\tilde{B}$ states of NO_2 with polar collision partners[27,28] and for a collision-induced intersystem crossing in SO_2.[29] Within this model, even with the aid of the giant ion-pair transition dipole, several further conditions have to be fulfilled to achieve the very large rates that we observed for H_2O. These can be deduced from the approximate expression for the critical impact parameter, b^*, at which the first order transition probability reaches 0.5. The dipole moment of water is perpendicular to the axis of largest B value (which defines the molecular z-axis, with μ then directed along the y-axis) and the dipole-dipole interaction energy requires a slight adaptation from the standard approach[30] to give

$$V_{12}=\frac{\mu_1\mu_2}{4\pi\varepsilon_0}R^{-3}\left(\sqrt{2}C_{10}(1)\{\mathcal{D}^1_{-10}(2)+\mathcal{D}^1_{10}(2)\}+\frac{1}{\sqrt{2}}C_{11}(1)\times\{\mathcal{D}^1_{-1-1}(2)+\mathcal{D}^1_{1-1}(2)\}+\frac{1}{\sqrt{2}}C_{1-1}(1)\{\mathcal{D}^1_{-11}(2)+\mathcal{D}^1_{11}(2)\}\right), \quad (5)$$

where the arguments of the spherical harmonics $C_{jm}(i)$ are the polar angles of the respective species, and $\mathcal{D}^J_{KM}$ is a matrix rotation element of the orientation of the water molecule with respect to the (moving) intermolecular axis, the index K referring to rotation of the y-axis about the molecule-fixed z-axis. Wave functions of a nearly prolate asymmetric top such as H_2O are either the symmetrized combinations $\mathcal{D}^J_{KM}\pm\mathcal{D}^J_{-KM}$ or linear combinations of them. Then, using first order time dependent perturbation theory with a constant velocity, v, and a rectilinear path with impact parameter, b, gives for the transition probability, $P_{J'_1J''_1J'_2J''_2}(b)$,

$$P_{J'_1J''_1J'_2J''_2}(b)=3\bar{S}_{I_2}(J'_1,J''_1)\bar{S}_{H_2O}(J'_2\tau',J''_2\tau'')\times\left\{\frac{2\kappa\langle v_g|\mu_{gu}|v_u\rangle\mu_{H_2O}}{4\pi\varepsilon_0\hbar vb^{*2}}e^{-(|\Delta E|b^*/\hbar v)}\right\}^2, \quad (6)$$

where ΔE is the overall internal energy change,

$$\Delta E=E_{I_2}(v_g,J'_1)+E_{H_2O}(J'_2\tau')-E_{I_2}(v_u,J''_1)+E_{H_2O}(J''_2\tau''), \quad (7)$$

where a single prime indicates an initial state and a double prime a final state and $\tau=K(\text{prolate})-K(\text{oblate})$. The $\bar{S}(J'_1J''_1)$ are Hönl–London factors for the rotational transitions resulting in ΔE, averaged over initial m states; they are identical for the three components of the field contributing to V_{12} in Eq. (5) and the factor 3 in Eq. (6) comes from summing the squares of the coefficients of these components. The path integral in the first order time dependent expression for the transition amplitude results in the Bessel function $K_1(\xi)$, where ξ is the Massey parameter $|\Delta E|b/\hbar v$ and κ in Eq. (6) is a numerical factor ~1, but weakly dependent on ξ, which comes from replacing $K_1(\xi)$ by $\kappa e^{-\xi}/\xi$ for small values of ξ (if $\Delta E=0$, $\kappa=1$).[31] This approximation recasts the expression for the transition probability into the same form as that for dipole/quadrupole coupling, when the factor μ_M is replaced by Θ_M/b, see Eq. (12).

For the high J values of I_2 the limiting value of $\bar{S}(J'_1J''_1)$ is 1/6 and this would also be the limiting value for H_2O at high J. However, if the more highly populated low J states of H_2O (typically $J'_2=0-5$, see Table III) are responsible for the quenching, $\bar{S}(J'_2\tau'J''_1\tau'')$ is both τ- and J-dependent. For example, for the transition $1_{-1}\rightarrow2_{-1}$ [for which $\Delta|K|=1$, as required by Eq. (5)] the m-averaged Hönl–London factor is 1/3, and for the $2_1\rightarrow2_{-1}$ transition the factor is 1/9.

In the measurements of g/u rate constants described above, the P and R branches were not resolved and the observed rates are the sum of these two channels. In the order of magnitude calculations of the inelastic collision cross sections to follow, we will take $2\times3\times\bar{S}(J'_1J''_1)\bar{S}(J'_2\tau'J'_2\tau'')$ to be 1/6.

For each initial rotational state of water, $(J'_2\tau')$, we define a critical impact parameter, b^*, at which, for a given $v'_1;J'_2\tau'\rightarrow v''_1;J''_2\tau''$ transition satisfies

$$\sum_{\Delta J=\pm1}\bar{P}^{(1)}_{\Delta J_1}\{b^*_{J'_2\tau'}(v'_1v''_1)\}=0.5, \quad (8)$$

for the sum of the first order probabilities $\bar{P}^{(1)}_{\Delta J_1}(b)$ for the P and R branches using the m_J-averaged Hönl–London coefficients for high J_1. Then the partial cross section for that pair of rovibrational channels and initial rotational state of water is

TABLE III. Energy gaps, ΔE_{I_2}, for the transitions from $f(v=6, \quad J=55)$ to various levels of the $F0_u^+(^3P_0)$ state, (F_v), the energy gaps, ΔE_{H_2O}, for the rotational transitions in H_2O, $J'_{\tau'} \rightarrow J''_{\tau''}$, that match these energy changes to within 5 cm^{-1} and the percentage of H_2O molecules at room temperature that are in the initial rotational level of these transitions, $\%(J'_{\tau'})$. Only the H_2O transitions in which $J'_{\tau'}$ has a rotational energy ≤ 500 cm^{-1} have been included, and only those for which $\Delta J=0, \pm 1$, $\Delta \tau=0, \pm 2$ as these characterize the strongest transitions.

I_2 $(f,v=6)$		H_2O		
F_v	ΔE_{I_2} $(J''=54/56)/cm^{-1}$	$\Delta E_{H_2O}/cm^{-1}$	$J'_{\tau'} \rightarrow J''_{\tau''}$	$J'_{\tau'}$ (%)
4	54.5/50.0	47	$5_{-3} \rightarrow 5_{-1}$	2.8
		53	$4_{-4} \rightarrow 4_{-2}$	1.7
		55	$2_{-1} \rightarrow 2_1$	5.9
		56	$1_{-1} \rightarrow 2_{-1}$	4.6
		57	$2_{-1} \rightarrow 3_{-3}$	4.5
5	−37.3/−41.9	33	$2_{-2} \rightarrow 1_0$	2.1
		37	$3_{-1} \rightarrow 3_{-3}$	5.3
		37	$1_0 \rightarrow 0_0$	1.5
		38	$3_{-1} \rightarrow 2_1$	5.3
		39	$3_1 \rightarrow 3_{-1}$	4.4
		40	$4_0 \rightarrow 4_{-2}$	1.1
		41	$2_2 \rightarrow 2_0$	1.5
6	−128.3/−132.8	127	$4_{-1} \rightarrow 3_{-1}$	3.7
		133	$3_1 \rightarrow 2_{-1}$	4.4

$$\sigma_{J'_2\tau'}(v'_1v''_1) = \sum_{P,R} \sigma_{J'_1J''_1J'_2J''_2}(v'_1v''_1) \simeq \pi b^*_{J'_2\tau'}(v'_1v''_1), \tag{9}$$

and the detailed rate constant is

$$k_{gu}(v'_1v''_1) \simeq \bar{v} \sum_{J'_2\tau'} W_{v'v''}(J'_2\tau')\sigma_{J'_2\tau'}(v'_1v''_1), \tag{10}$$

where $W_{v'v''}(J'_2\tau')$ is the fractional population of the initial rotational state of water that leads to rotational transitions in resonance with $v' \rightarrow v''$ in the ion-pair state to within $|\Delta E|$ cm^{-1} (see Table III). The exponential factor in Eq. (6) is of paramount importance in determining the value of $|\Delta E|$ that, given the other parameter values, yields a value of b^* that leads to a final rate constant of the required magnitude. Taking $\langle v_g|\mu_{gu}(R)|v_u\rangle = 3.5$ eÅ $\times \langle v_g|v_u\rangle$, a FCF $\langle v_g|v_u\rangle^2 = 0.5$, $\mu_{H_2O} = 0.38$ eÅ, the product of the Hönl–London factors to equal 1/6 and $b^* = 20$ Å, we find $|\Delta E| \sim 5$ cm^{-1}, and $b^* = 30$ Å requires $|\Delta E| \sim 2$ cm^{-1}.

Clearly these are very demanding requirements for energy matching and we look to see if the IR absorption spectrum of H_2O offers strong transitions that fulfill these conditions for the vibrational distributions observed in the $f0_g^+(^3P_0)$ and $E0_g^+(^3P_2)$ state fluorescence spectra (for inducing an exothermic transition the initial and final states for absorption are of course reversed, together with their Boltzmann factors). It can be seen from Table I that the required transition energies in H_2O must range from 17 to 170 cm^{-1} to produce resonances with the most populated final vibrational levels of the $F0_u^+(^3P_0)$ state and up to 270 cm^{-1} for the $E0_g^+(^3P_2)$ state distributions.

The first point to note is that, since H_2O is not a symmetric top, dipole-dipole coupling must be accompanied by a change in rotational energy and the lowest allowed transitions are at 15 cm^{-1} $(5_4 \leftrightarrow 6_2)$ and 18 cm^{-1} $(1_1 \leftrightarrow 1_{-1})$. Thus, H_2O cannot induce the transition $f(v=10) \rightarrow F(v=9)$ in either the P branch $(\Delta E_{I_2} = 5.5$ $cm^{-1})$ or the R branch $(\Delta E_{I_2} = 0.9$ $cm^{-1})$ because the lowest overall internal energy change, $\Delta E = |\Delta E_{I_2} + \Delta E_{H_2O}|$ would be 10 cm^{-1}, outside the narrow energy mismatch required to compensate for the relatively small FCF of 3×10^{-3}. There is thus no peak in the rate constant for water as the collision partner at $f(v=10)$ (Fig. 6). In contrast with $I_2(X)$ as the collision partner, the very small B value of I_2 means that the required $\Delta J=0$ or ± 2 change for quadrupole/dipole coupling requires so little energy in $I_2(X)$ (0 or $\sim 4JB_X$) that the overall value of ΔE as defined in Eq. (7) remains within 5 cm^{-1} for a wide range of J values of the collision partner, which helps compensate for the small FCF. Consequently, the self-quenching of $E(v=13)$ is almost exclusively to the nearly isoenergetic $D(v=18)$ (Table I), but this transition is completely absent with H_2O as the collision partner.

With H_2O as the collision partner, in *every* case where the population of a final vibrational state is ≥ 0.1, the required change in the ion-pair state can be matched in either one or both of the rotational branches to within 5 cm^{-1}, and usually to within 2 cm^{-1}, by several strong rotational transition in H_2O. We illustrate this with the vibrational levels in the $F0_u^+(^3P_0)$ state that are observed to be populated from $f(v=6)$ by collisions with H_2O. Rotational transitions in H_2O that match these energy changes to within 5 cm^{-1} are given in Table III. The smaller energy changes in the ion-pair state, 30–60 cm^{-1}, are matched more densely than those above 100 cm^{-1} by rotational transitions in H_2O, and in addition the lower energy transitions involve the more populated lower rotational states. It can be seen from Table III that the total percentage of H_2O molecules at room temperature that are in the initial rotational levels of the these transitions, $W_{v'v''}$, for the $f(v=6) \rightarrow F$ $(v=4$ and $5)$ transitions is $\sim 20\%$ but is only $\sim 8\%$ for the $f(v=6) \rightarrow F(v=6)$ transition where larger ΔE changes are involved. However, the $f(v=6) \rightarrow F(v=6)$ transition has an order of magnitude larger FCF and the result is an almost equal population of F $(v=5$ and $6)$. The $F(v=4)$ level is less well populated than the $F(v=5)$ level even though an equal number of strongly resonant transitions are available; the smaller FCF is clearly beginning to reduce the transition rate. Exactly the same propensities can be found in the final vibrational state distributions derived from all the initial vibrational levels of the $f0_g^+(^3P_0)$ and $E0_g^+(^3P_2)$ states that we studied.

The requirement $\Delta E \leq 5$ cm^{-1} (and preferably ≤ 2 cm^{-1} if a final vibrational level is to be populated by H_2O with a detailed rate constant $\geq 100 \times 10^{-10}$ $molecules^{-1}$ cm^3 s^{-1}) suggests that the P and R branch intensities resulting from transitions from a common initial state may well be very unequal. This will become more likely as the branch separation increases at higher J values, and also as the resonant transitions required from H_2O move to higher energies where the density of far-IR lines is less. Even in the case of the collision induced transitions $f(v=6, J=55) \rightarrow F(v=6, \quad J=54/56)$ where the branch separation (see Table III) is ~ 4.5 cm^{-1}, the two rotational transitions in H_2O that are responsible for the resonances effectively only

control one branch each, being 5 cm^{-1} off-resonance for the neighboring transition. These two rotational transitions in H_2O will not have the same intensity, partly because they originate in J states ($J=3$ and $J=4$) with different parities, the odd-J states being weighted three times the even-J states.

In the present experiments we collect emission from the $D0_u^+(^3P_2)$ and $F0_u^+(^3P_0)$ ion-pair states to the ground state, each vibronic band of which is comprised of four lines, a P and R branch from each of the two collisionally populated rotational levels. Although we are unable to resolve any rotational structure, it was shown in an earlier study by Inard *et al.*[14] that similar emission could be resolved using Fourier transform detection. It would be interesting to see, using this technique, if the line intensities in the presence, intentional or otherwise, of H_2O vapor follow the model presented here.

2. $I_2(X)$

The coupling potential between the transition dipole in the ion-pair states $\mu_{gu}^{(1)}$ and the permanent quadrupole moment $\Theta_{zz}^{(2)}$ of ground-state iodine is

$$V^{(3)} = \frac{3}{R^4}\mu_{gu}^{(1)}\Theta_{zz}^{(2)}\left(C_{10}(1)C_{20}(2) - \frac{1}{\sqrt{3}}C_{11}(1)C_{2\text{-}1}(2) - \frac{1}{\sqrt{3}}C_{1\text{-}1}(1)C_{21}(2)\right). \quad (11)$$

The transition amplitude for $v_1'J_1';J_2' \rightarrow v_1''J_1'';J_2''$ for a collision with relative velocity v and impact parameter b is

$$a_{J_1'J_1''J_2'J_2''}(b) = \frac{3\pi\mu_{gu}^{(1)}\Theta_{zz}^{(2)}}{2\hbar v b^3}\langle v_1'|v_1''\rangle \bar{S}_{J_1'J_1''}\bar{S}_{J_2'J_2''}[1+\xi]e^{-\xi}, \quad (12)$$

where ξ is the Massey parameter defined above and the $\bar{S}_{J'J''}$ factors are the appropriate combination of m_J-averaged Heitler–London factors for the parallel and perpendicular transitions weighted as in Eq. (11), each of which describes a different scattering channel. The $\bar{S}_{J_2'J_2''}$ for the $I_2(X)$ collision partner are the squares of the rotational matrix elements of the quadrupolar transitions in Eq. (11) and the m_J averaging is carried out in the high-J limit.

Once again, the energy mismatch ΔE plays a vital role in determining whether long-range coupling can enhance the inelastic cross section. The observed rate for $f(v=10) \rightarrow F(v=9)$ is 8×10^{-10} molecules^{-1} cm^3 s^{-1} and with a relative collision velocity of 2.2×10^4 cm s^{-1} this implies a critical impact parameter $b^* \sim 11$ Å at which the transition probability reaches 0.5. The ΔE values for the two rotational branches of the final ion-pair state, 5.5 and 0.9 cm^{-1}, are at their minimum for this vibrational transition but the FCF $\langle v_1'|v_1''\rangle^2$ is only 3×10^{-3} and we now see if dipole-quadrupole coupling can account for the observed rate.

The $C_{2m}(2)$ terms in Eq. (11) can induce either $\Delta J_2=0$ or ±2 transitions in the ground state collision partner, associated with energy changes of 0 and $\sim 4JB_X$, respectively; at room temperature the most highly populated rotational level, J_{max}, is $\sim$50 and $4JB_X \sim 8$ cm^{-1}. The product of Heitler–London factors associated with $\Delta J_2=0$, averaged over all m_1' and m_2' states and summed over the $\Delta J_1''$ branches (which are not resolved) is 3.9×10^{-2}, and 8.3×10^{-2} for the $\Delta J_2=\pm2$ transitions. Taking $\Theta_{zz}^{(2)}=23\times10^{-40}$ C m^2,[32,33] to achieve a critical impact parameter $\gtrsim$11 Å then requires $\Delta E \lesssim 2.5$ cm^{-1} for both $\Delta J_2=0$ and ±2 rotational changes in $I_2(X)$. Thus if there is no change in the rotational energy of $I_2(X)$, the P branch ($\Delta E=0.9$ cm^{-1}) of the ion-pair transition can be excited, and the $\Delta J_2=+2$ transition in the collision partner can just excite the R branch ($\Delta E=5.5$ cm^{-1}) in a resonant fashion to achieve the observed transition rate.

B. Comparison with previous studies of collisional transfer by $I_2(X)$

The published vibrational distributions and rate constants for those vibrational levels that we also studied are included in Tables I and II. All of the discrepancies in the vibrational distributions can be attributed to varying concentrations of residual H_2O in the cell, probably up to 0.03 Torr, in the previous studies.[2–12] For example, the $f(v=12)$ spectrum shown in the upper trace of Fig. 2(b), which contains a contribution from desorbed H_2O, was simulated with a vibrational distribution in the $F0_u^+(^3P_0)$ state, $N_{10}:N_{11}:N_{12}:N_{13}$, of 0.2:1:0.7:0.1. An almost identical distribution was reported previously[2] and attributed to collisional transfer by $I_2(X)$ alone. Using the rate constants and vibrational distributions measured in the present work, this vibrational distribution corresponds to there being approximately 15 mTorr of desorbed H_2O in the cell in both experiments. All of the other reported vibrational distributions[2,9] are also consistent with the presence of a similar H_2O pressure.

In contrast, the presence of H_2O cannot entirely explain the discrepancies in the rate constants for "pure" I_2. A plot of total rate constants for a sample that consists of 0.2 Torr of I_2 and 15 mTorr of desorbed H_2O, calculated from the values obtained in the present work and presented in Table II, against v will show a peak, centered on $f(v=10)$, on a monotonically rising background. Qualitatively, this was observed in an earlier study.[2] However, the reported values[2] are all two to three times greater than those calculated in this way, i.e., the differences lie outside the combined quoted uncertainties. There is an analogous discrepancy in the $E0_g^+(^3P_2)$ state data. We have no explanation for these differences.

We found a rate constant of only 0.2×10^{-10} molecules^{-1} cm^3 s^{-1} for transfer from one nonresonant level of the $E0_g^+(^3P_2)$ state, $v=8$. This is compatible with a value of 0.4×10^{-10} molecules^{-1} cm^3 s^{-1} reported for $v=0$ of the $E0_g^+(^3P_2)$ state[13] from a research group where the authors reported that the cell was evacuated to 2×10^{-5} Torr and so any concentration of H_2O must be negligible. Although there is fairly good energy matching in the latter case, E_{I_2} for $E0_g^+(v=0) \rightarrow D0_u^+(v=4) \sim 10$ cm^{-1}, the FCF for this transition is only 2×10^{-5} and long range coupling would not be expected for self-quenching.

VI. CONCLUSIONS

It has been shown that an impurity, which could be present in some of the work done by two other research groups, could significantly affect the rate constants for transfer between ion-pair states of I_2. The evolution in time of the

product vibrational distribution suggests that the contaminant is H_2O, desorbing from the walls of the cell. Very large rate constants are measured from Stern–Volmer plots for collisional transfer by H_2O, up to 50×10^{-10} molecules^{-1} cm^3 s^{-1}, from a range of vibrational levels of the $f0_g^+(^3P_0)$ state. Collisions with H_2O also lead to a characteristic vibrational distribution in the final electronic state that is quite different from that produced by $I_2(X)$ as the collision partner and this served as a fingerprint for the presence of water that can be seen in the other studies. A model for parity change by water as the collision partner has been proposed in which long-range, near-resonant interactions can occur when there is close matching, to within 5 cm^{-1}, of the change in energy in the ion-pair states with the energy of selective rotational transitions in the collision partner. We have further shown that, using simple first order perturbation theory, this long range dipole-dipole coupling can result in the very large observed rates with water even allowing for the reduced population of resonant rotational states.

We repeated some previously reported studies on the $f0_g^+(^3P_0)\rightarrow F0_u^+(^3P_0)$ and $E0_g^+(^3P_2)\rightarrow D0_u^+(^3P_2)$ collisional transfer by $I_2(X)$, taking care to reduce the H_2O concentration to the minimum possible level, and extended the vibrational range covered. Much lower rate constants than those previously reported are found, with only one vibrational level of the initial ion-pair state exhibiting a resonant enhancement. In this case, the dipole-quadrupole long-range coupling model is shown to be applicable because the internal energy matching of the initial and final states is within 5 cm^{-1} for a wide range of rotational states of the collision partner.

The rates for collisional transfer by $I_2(X)$ are one or two orders of magnitude smaller than those for H_2O, so even very low concentrations of H_2O can seriously impact on studies with apparently pure I_2 that appeared in the literature. The presence of H_2O, however, should not adversely affect studies of transition rates with other collision partners that are obtained by subtracting from the total emission the contribution from collisions with $I_2(X)$ measured under local conditions, and it does not matter if the latter contains a contribution from collisions with H_2O.

ACKNOWLEDGMENTS

We would like to thank Dr. V. Alekseev for numerous stimulating discussions.

[1] T. Ridley, K. P. Lawley, and R. J. Donovan, J. Chem. Phys. **130**, 124302 (2009).
[2] M. E. Akopyan, I. Y. Chinkova, T. V. Fedorova, S. A. Poretsky, and A. M. Pravilov, Chem. Phys. **302**, 61 (2004).
[3] M. E. Akopyan, N. K. Bibinov, D. B. Kokh, A. M. Pravilov, M. B. Stepanov, and O. S. Vasyutinskii, Chem. Phys. **242**, 263 (1999).
[4] M. E. Akopyan, N. K. Bibinov, D. B. Kokh, A. M. Pravilov, O. L. Sharova, and M. B. Stepanov, Chem. Phys. **263**, 459 (2001).
[5] N. K. Bibinov, O. L. Malinina, A. M. Pravilov, M. B. Stepanov, and A. A. Zakharova, Chem. Phys. **277**, 179 (2002).
[6] T. V. Tscherbul, A. A. Buchachenko, M. E. Akopyan, S. A. Poretsky, A. M. Pravilov, and T. A. Stephenson, Phys. Chem. Chem. Phys. **6**, 3201 (2004).
[7] M. E. Akopyan, I. Y. Novikova, S. A. Poretsky, A. M. Pravilov, A. G. Smolin, T. V. Tscherbul, and A. A. Buchachenko, J. Chem. Phys. **122**, 204318 (2005).
[8] M. E. Akopyan, A. A. Buchachenko, S. S. Lukashov, S. A. Poretsky, A. M. Pravilov, Y. V. Suleimanov, A. S. Torgashkova, and T. V. Tscherbul, Chem. Phys. Lett. **436**, 1 (2007).
[9] M. E. Akopyan, S. S. Lukashov, E. I. Khadikova, E. A. Nikandrova, S. A. Poretsky, A. M. Pravilov, and A. S. Torgashkova, Chem. Phys. **342**, 173 (2007).
[10] M. E. Akopyan, S. S. Lukashov, Y. D. Maslennikova, S. A. Poretsky, A. M. Pravilov, and A. S. Torgashkova, Chem. Phys. Lett. **458**, 29 (2008).
[11] W. Ubachs, I. Aben, J. B. Milan, G. J. Somsen, A. G. Stuiver, and W. Hogervorst, Chem. Phys. **174**, 285 (1993).
[12] R. Teule, S. Stolte, and W. Ubachs, Laser Chem. **18**, 111 (1999).
[13] C. J. Fecko, M. A. Freedman, and T. A. Stephenson, J. Chem. Phys. **115**, 4132 (2001).
[14] D. Inard, D. Cerny, M. Nota, R. Bacis, S. Churassy, and V. Skorokhodov, Chem. Phys. **243**, 305 (1999).
[15] R. Martin, R. Bacis, S. Churassy, and J. Vergès, J. Mol. Spectrosc. **116**, 71 (1986).
[16] P. Luc, J. Mol. Spectrosc. **80**, 41 (1980).
[17] J. Tellinghuisen, J. Mol. Spectrosc. **217**, 212 (2003).
[18] J. C. D. Brand, A. R. Hoy, A. K. Kalkar, and A. B. Yamashita, J. Mol. Spectrosc. **95**, 350 (1982).
[19] J. P. Perrot, A. J. Bouvier, A. Bouvier, B. Femelat, and J. Chevaleyre, J. Mol. Spectrosc. **114**, 60 (1985).
[20] T. Ishiwata, T. Kusayanagi, T. Hara, and I. Tanaka, J. Mol. Spectrosc. **119**, 337 (1986).
[21] M. E. Akopyan, N. K. Bibinov, D. B. Kokh, A. M. Pravilov, and M. B. Stepanov, Chem. Phys. **242**, 253 (1999).
[22] M. E. Akopyan, I. Y. Novikova, S. A. Poretsky, A. M. Pravilov, A. G. Smolin, and T. V. Fedorova, Opt. Spectrosc. **99**, 36 (2005).
[23] T. Ridley, K. P. Lawley, and R. J. Donovan, Chem. Phys. **348**, 227 (2008).
[24] K. P. Lawley, P. J. Jewsbury, T. Ridley, P. R. R. Langridge-Smith, and R. J. Donovan, Mol. Phys. **75**, 811 (1992).
[25] J. P. Perrot, B. Femelat, J. L. Subtil, M. Broyer, and J. Chevaleyre, Mol. Phys. **61**, 85 (1987).
[26] K. P. Lawley, Chem. Phys. **127**, 363 (1988).
[27] G. V. Hartland, D. Qin, and H.-L. Dai, J. Chem. Phys. **102**, 8677 (1995).
[28] G. V. Hartland, D. Qin, H.-L. Dai, and C. Chen, J. Chem. Phys. **107**, 2890 (1997).
[29] M. Zhang and H.-L. Dai, J. Phys. Chem. A **111**, 9632 (2007).
[30] R. D. Sharma and C. A. Brau, J. Chem. Phys. **50**, 924 (1969).
[31] G. N. Watson, *A Treatise on the Theory of Bessel Functions* (Cambridge University Press, Cambridge, 1966).
[32] C. Graham, D. A. Imrie, and R. E. Raab, Mol. Phys. **93**, 49 (1998).
[33] A. J. Alexander and T. P. Rakitzis, Mol. Phys. **103**, 1665 (2005).